Gate-defined double quantum dot with integrated charge sensors realized in InGaAs/InP by incorporating a high-κ dielectric

Jie Sun[a], Marcus Larsson, Ivan Maximov, and H. Q. Xu[b]
Division of Solid State Physics, Lund University, Box 118, S-22100 Lund, Sweden
(Dated: June 4, 2012)

Gate-defined double quantum dots with integrated quantum point contact charge sensors are realized in an InGaAs/InP heterostructure by employing a high-κ HfO_2 thin film as gate dielectric and a polymer bridge technique. Clear honeycomb patterns are observed in the measured charge stability diagram of the double quantum dots and charge sensing signals of the quantum point contacts. It is also found that the quantum point contact charge sensors can detect the charge states in the double quantum dots even in the condition that the direct transport signal is not visible.

Semiconductor double quantum dots (QDs) have been extensively investigated in recent years due to an increasing interest in the studies of the fundamental physics revealed in such artificial molecular systems and in the developments of nanoelectronic logic gates and solid state based devices for quantum information processing and computation.[1] In these studies and developments, it is desired that spin states, spin procession, and spin interactions can be tuned in a controlled manner.[2] Double QDs can be realized by employing metal gates on top of a semiconductor heterostructure hosting a high-mobility two-dimensional electron gas (2DEG).[3] Highly tunable QDs with smooth boundaries are achieved by this top-gate technology in GaAs/AlGaAs heterostructures.[3–6] However, gate-defined double QDs in InGaAs/InP heterostructures have not been reported. The 2DEG in an InGaAs/InP heterostructure has interesting electron transport properties, such as small electron effective mass, high electron mobility, large effective g-factor, and strong spin-orbit coupling strength.[7–10] Thus, it is of great interest to employ double QD devices defined in InGaAs/InP for study of spin physics and for development of spin-qubit entangled devices. Nevertheless, there exists a technical obstacle in applying the standard top-gates technology to an InGaAs/InP heterostructure due to a low Schottky barrier formed in the interface between a metal and heterostructure surface.[11,12]

In this letter, we report on realization of a gate-defined double QD device in an InGaAs/InP heterostructure by using HfO_2 as gate dielectric and a polymer bridge technique. The employment of the high-κ material reduced the gate leakage current without significantly reducing the gate efficiency.[8] A cross-linked polymethylmethacrylate (PMMA) was employed as the supporting material to the bridge. The double QD device was integrated with two quantum point contacts (QPCs) as charge sensors.[4,13,14] The electron transport measurements showed that the double QD was highly tunable and typical honeycomb patterns were observed in the charge stability diagram. The charge states in the double QD were even more clearly detected by the two QPC charge detectors, indicating realization of a double QD device with a sensitive charge readout scheme in the InGaAs/InP heterostructure.

The device studied in this work was fabricated from a modulation-doped InGaAs/InP heterostructure grown by metal-organic vapor phase epitaxy.[7,15] On a semi-insulating InP substrate, a 50 nm undoped InP buffer layer, a 9 nm $In_{0.75}Ga_{0.25}As$ quantum well, a 20 nm undoped InP layer, a 1 nm Si δ-doped InP layer, and finally a 20 nm InP cap layer were successively grown. At

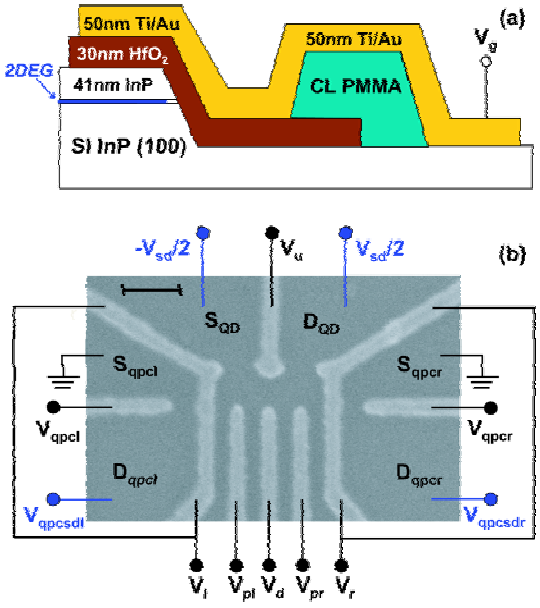

FIG. 1: (Color online) (a) Schematic diagram showing the cross section of a device, where InGaAs/InP heterostructure, HfO_2 film, Ti/Au gate and cross-linked PMMA material are indicated. A negative voltage V_g can be applied to the Ti/Au gate to deplete the 2DEG beneath. (b) Scanning electron microscope (SEM) image of the central part of the device studied in this work (top view) and measurement circuit setup. The scale bar is 200 nm.

[a] Present address: MC2, Chalmers University of Technology, S-41296 Gothenburg, Sweden.
[b] Author to whom correspondence should be addressed. Electronic mail: hongqi.xu@ftf.lth.se.

300 mK, the sheet concentration, mobility and mean free path of the 2DEG formed in the InGaAs quantum well were determined, by Hall measurements in dark, to be 4.2×10^{15} m^{-2}, 6.77 m^2/Vs, and 725 nm, respectively. On mesas with Au/Ge ohmic contacts, a 30 nm thick HfO_2 film was grown from $Hf[N(CH_3)_2]_4$ and H_2O by atomic layer deposition (ALD) at 100 ^oC. The permittivity κ of the grown HfO_2 film was estimated to be 16.6.[16] A lift-off technique was used to pattern the HfO_2 film, where ZEP 520A-7 resist was employed. Using very high dose (30000 $\mu C/cm^2$) electron beam lithography (EBL), PMMA 950A6 resist was locally cross-linked at the edges of the HfO_2 film, serving as bridge supporter [see Fig. 1(a)]. Finally, the top gates were fabricated by single pixel line EBL and thermal evaporation of 50 nm Ti/Au. Here, we note that an oxide directly grown onto InP can result in electrical instabilities at the oxide/InP interface.[17] By employing the PMMA bridge, the gate contact bonding pads can be placed outside of the HfO_2 coverage area, as indicated in Fig. 1(a). Thus, any direct electrical connection between the bonding wires and a parasitic charge accumulation layer possibly formed at the HfO_2/InP interface can be avoided.

A fabricated InGaAs/InP double QD device with two integrated QPC charge detectors is shown in Fig. 1(b). The QDs had a lithographically defined diameter of ~150 nm. The device had 6 ohmic contacts: the double QD source and drain contacts S_{QD} and D_{QD}, the left QPC source and drain contacts S_{qpcl} and D_{qpcl}, and the right QPC source and drain contacts S_{qpcr} and D_{qpcr}. In the measurements, a voltage V_{sd} was applied to the source and drain contacts of the double QD in an antisymmetrical way as shown in Fig. 1(b). voltages V_{qpcsdl} and V_{qpcsdr} were applied to the two QPC drain contacts, while the two QPC source contact S_{qpcr} and S_{qpcr} were kept grounded. The device contained 8 top gates, see Fig. 1(b). The double dot was defined by voltages V_u and V_d applied to the upper and lower barrier gates, and voltages V_l and V_r to the left and right barrier gates. Voltages V_{pl} and V_{pr} applied to the left and right plunger gate were used to tune the electron numbers in the QDs. The two additional gates with applied voltages V_{qpcl} and V_{qpcr} were used to define and tune the left and right QPCs. The integrated device was cooled down to 300 mK in a ^{3}He cryostat for transport measurements.

Figure 2 shows the measured current I_{sd} through the double QD as a function of voltages V_{pl} and V_{pr} applied to the left and right plunger gates at a small bias voltage of $V_{sd} = 50$ μV (a charge stability diagram). Here, the double dot was defined by setting gate voltages at $V_u = -1.63$ V, $V_d = -1.93$ V, $V_l = -1.49$ V and $V_r = -1.8$ V, and the two QPCs were not in use. A honeycomb pattern typical for a double QD device[18] is seen in the stability diagram shown in Fig. 2. Assume that there is no cross capacitance between a plunger gate and the QD which is capacitively coupled to the other plunger gate. Then, for completely decoupled QDs (i.e., without quantum mechanical tunneling between the two

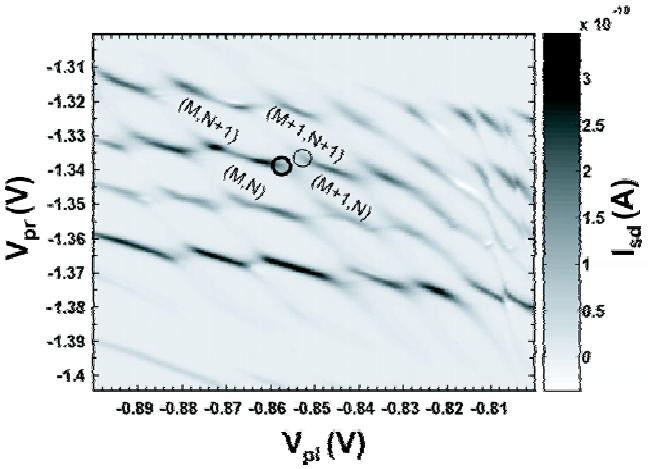

FIG. 2: (Color online) Source-drain current I_{sd} measured for the double QD device, at a small bias of V_{sd}=50 μV, as a function of plunger gate voltages V_{pl} and V_{pr} (a charge stability diagram). Two typical triple points are marked with a thick and a thin circle, and a few charge states are indicated by integer numbers in parentheses (M,N), where M stands for number electron in the left QD and N the number of electrons in the right QD.

QDs), the domain of a charge state of the double QD is in a square shape (for a symmetric double QD device) or a rectangular shape (for an asymmetric double QD device). Hexagons appear when the interdot coupling is increased. In the extreme case where the coupling is so large that the two QDs merge into one big dot, charge state domains turn to be defined by straight parallel lines. The charge stability diagram shown in Fig. 2 indicates that the double QD was in the intermediate interdot coupling regime, where the interdot tunnel barrier was transparent enough to allow for a current and was opaque enough for defining the number of electrons in each QD. At every triple point of the honeycomb structure shown in Fig. 2, the electrochemical potentials of the two QDs (at different charge states) are aligned to the Fermi level of the source and drain of the double QD in such a way that electrons can be shuttled from the left to the right through the double QD. For example, at the triple point marked with a thick circle in Fig. 2, three double-QD charge states (M, N), $(M + 1, N)$ and $(M, N + 1)$ become degenerate and the electrochemical potentials in the left QD, $\mu_l(M, N)$ and $\mu_l(M + 1, N)$, and the right QD, $\mu_r(M, N + 1)$ and $\mu_r(M, N)$, are all aligned with the Fermi levels of the double-QD source and drain contacts, $\mu_s = \mu_l(M, N) = \mu_l(M + 1, N) = \mu_r(M, N + 1) = \mu_r(M, N) = \mu_d$, where M and N represent the numbers of electrons in the left and the right QD, respectively. Thus, electrons can tunnel through the double QD in the sequence of $(M, N) \rightarrow (M + 1, N) \rightarrow (M, N+1) \rightarrow (M, N)$. At the triple point marked with a thin circle in Fig. 2, double-QD charge states $(M+1, N)$, $(M, N + 1)$ and $(M + 1, N + 1)$ are degenerate and electrons can tunnel through the double QD in the sequence

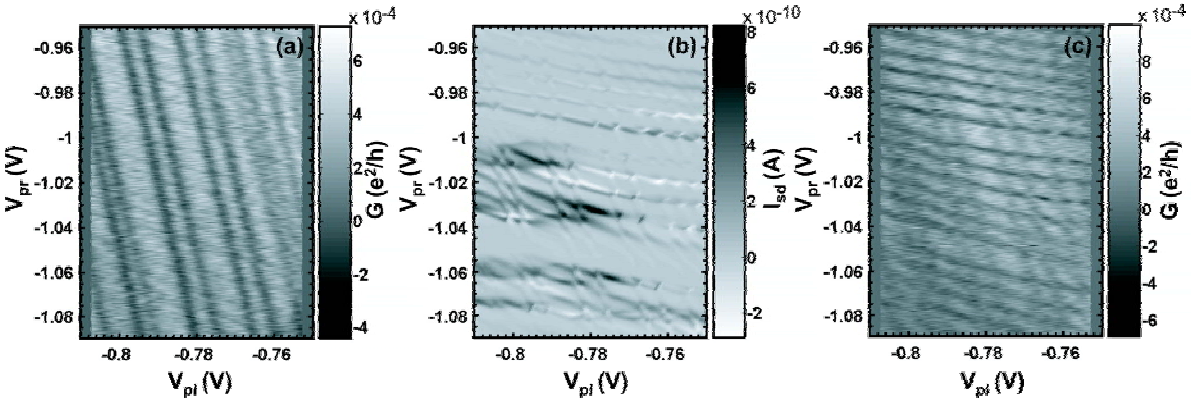

FIG. 3: (Color online) Charge sensing experiment. Here, the data shown in (a), (b), and (c) were measured simultaneously. (a) Transconductance $\partial I_{QPCsdl}/\partial V_{pl}$ (charge sensing signal) of the left QPC, (b) source-drain current I_{sd} measured for the double QD device under a small bias of V_{sd}=50 μV (a charge stability diagram), and (c) transconductance $\partial I_{QPCsdr}/\partial V_{pl}$ (charge sensing signal) of the right QPC. In the measurements, V_{pl} was swept, while V_{pr} was stepped.

of $(M+1, N+1) \rightarrow (M+1, N) \rightarrow (M, N+1) \rightarrow (M+1, N+1)$, which can also be considered as that holes are transfered through the double QD from the right to the left. Ideally, the two types of triple points form two square lattices. However, with finite cross capacitances, the positions of the triple points move to lower V_{pl} (V_{pr}) for increasing V_{pr} (V_{pl}).[18] At the borders of the hexagons, the electrochemical potential in one QD is aligned to the source and drain electrochemical potentials μ_s and μ_d, while the electrochemical potential in the other QD is misaligned to μ_s and μ_d. Transport can take place through co-tunneling via a virtual state.[19] From the geometry of the hexagonal cells, the plunger gate capacitances can be calculated through $C_{pl(pr)} = e/\Delta V_{pl(pr)}$. For example, from the (M, N) cell in Fig. 2, we obtained $C_{pl} \approx 8.65$ aF and $C_{pr} \approx 11.4$ aF.

Figure 3 presents the data of our charge-sensing measurements. The device was defined by setting gate voltages at $V_u = -1.75$ V, $V_d = -2.15$ V, $V_l = -1.5$ V, $V_r = -1.67$ V, $V_{qpcl} = -1.975$ V and $V_{qpcr} = -1.7$ V. The measurements were taken at the bias voltage of $V_{sd} = 50$ μV to the double QD and the bias voltages of $V_{qpcsdl} = V_{qpcsdr} = 100$ μV to the left and right QPCs. At this working voltage configuration, the QPCs were very sensitive to a potential shift in the environment and the transconductances $\partial I_{QPCsdl}/\partial V_{pl}$ and $\partial I_{QPCsdr}/\partial V_{pr}$ as high as ~112 nS could be detected. Here, I_{QPCsdl} and I_{QPCsdr} stand for the currents passing through the left and right QPCs. Figure 3(b) depicts a measured charge stability diagram of the double QD, where a large number of hexagonal cells are seen. Here, it is seen that the source-drain current peaks are more pronounced at some plunger gate voltages than at others. This irregularity in the peak amplitude of current is mainly due to the variations in the QD-2DEG reservoir couplings and in the interdot coupling.[20,21] Figure 3(a) shows the simultaneously measured response signal of the left QPC, where the transconductance $\partial I_{QPCsdl}/\partial V_{pl}$ of the QPC is plotted as a function of V_{pl} and V_{pr}. Here, a change in the electron number in the double QD are reflected by the negative peaks in the transconductance. Figure 3(c) shows the simultaneously measured transconductance $\partial I_{QPCsdr}/\partial V_{pl}$ of the right QPC. Here, the same honeycomb structure as in Fig. 3(a) is found. However, the signal strengths in Figs. 3(a) and 3(c) are not identical due to the asymmetric capacitive couplings between the QDs and QPCs. The left QPC detects single electrons in the left QD more effectively than in the right QD. Therefore, in Fig. 3(a), the vertical lines are stronger than the horizontal lines. In a similar manner, a more effective sensing of single electrons in the right QD is observed in Fig. 3(c). The amplitude variations in current peak seen in Fig. 3(b) are, however, not reproduced in Figs. 3(a) and 3(c), signifying that the QPCs detected the charge states rather than the charging process. Furthermore, charge states of the double QD were also clearly detected by the two QPCs in the gate voltage regions where the direct transport signal was hardly visible, indicating that the complementary measurement signals of the two QPCs provided highly sensitive detection of the electron charges in the double QD.

In summary, we have developed a top-gate technology for fabrication of quantum devices in InGaAs/InP heterostructures. HfO_2 thin film has been incorporated as gate dielectric and a PMMA bridge technique has been employed to avoid electrical connection between the contact pads and parasitic charge accumulation layer which could possibly formed at the HfO_2/InP interface. The technology has been exploited to realize gate-defined double QD devices with integrated QPC charge sensors in an InGaAs/InP heterostructure. Direct transport measurements show Coulomb blockade honeycomb patterns typical for a double QD device. It has also been found that QPCs can effectively detect the electron charge states of the double QD even when direct transport signal becomes hardly visible. The results of this work should stimulate

realization of spin and quantum devices in materials systems other than GaAs/AlGaAs heterostructures, where the application of gating technology has been difficult.

This work was supported by the Swedish Research Council (VR) and by EU program SUBTLE (EU Contract No. 034236).

[1] D. DiVincenzo, Science **309**, 2173 (2005).
[2] D. Loss and D. DiVincenzo, Phys. Rev. A **57**, 120 (1998).
[3] J. Petta, A. Johnson, J. Taylor, E. Laird, A. Yacoby, M. Lukin, C. Marcus, M. Hanson, and A. Gossard, Science **309**, 2180 (2005).
[4] T. Fujisawa, T. Hayashi, R. Tomita, and Y. Hirayama, Science **312**, 1634 (2006).
[5] F. Koppens, J. Folk, J. Elzerman, R. Hanson, L. Willems van Beveren, I. Vink, H. Tranitz, W. Wegscheider, L. Kouwenhoven, and L. Vandersypen, Science **309**, 1346 (2005).
[6] M. Pioro-Ladriere, M. Ciorga, J. Lapointe, P. Zawadzki, M. Korkusinski, P. Hawrylak, and A. Sachrajda, Phys. Rev. Lett. **91**, 026803 (2003).
[7] P. Ramvall, N. Carlsson, P. Omling, L. Samuelson, W. Seifert, M. Stolze, and Q. Wang, Appl. Phys. Lett. **68**, 1111 (1996).
[8] J. Sun, M. Larsson, I. Maximov, H. Hardtdegen, and H. Q. Xu, Appl. Phys. Lett. **94**, 042114 (2009).
[9] M. Larsson, H. Nilsson, H. Hardtdegen, and H. Q. Xu, Appl. Phys. Lett. **95**, 192112 (2009).
[10] T. Koga, J. Nitta, T. Akazaki, and H. Takayanagi, Phys. Rev. Lett. **89**, 046801 (2002).
[11] A. Ahaitouf, E. Losson, and A. Bath, Solid State Electron. **44**, 515 (2005).
[12] H. Cetin and E. Ayyildiz, Semicond. Sci. Technol. **20**, 625 (2005).
[13] E. Sukhorukov, A. Jordan, S. Gustavsson, R. Leturcq, T. Ihn, and K. Ensslin, Nature Phys. **3**, 243 (2007).
[14] D. Wallin, A. Fuhrer, L. E. Froberg, L. Samuelson, H. Q. Xu, S. Hofling, and A. Forchel, Appl. Phys. Lett. **90**, 172112 (2007).
[15] I. Shorubalko, H. Q. Xu, I. Maximov, P. Omling, L. Samuelson, and W. Seifert, Appl. Phys. Lett. **79**, 1384 (2001).
[16] J. Sun, E. Lind, I. Maximov, and H. Q. Xu, unpublished.
[17] J. Wager, K. Geib, C. Wilmsen, and L. Kazmerski, J. Vac. Sci. Technol. B **1**, 778 (1983).
[18] W. van der Wiel, S. De Franceschi, J. Elzerman, T. Fujisawa, S. Tarucha, and L. Kouwenhoven, Rev. Mod. Phys. **75**, 1 (2003).
[19] D. V. Averin and Yu. V. Nazarov, in *Single Charge Tunneling: Coulomb Blockade Phenomena in Nanostructures*, edited by H. Grabert and M. H. Devoret (Plenum Press, New York and London, 1992), p. 217.
[20] M. Stopa, Phys. Rev. B **48**, 18340 (1993).
[21] M. Larsson, D. Wallin, and H. Q. Xu, J. Appl. Phys. **103**, 086101 (2008).